Available online at www.sciencedirect.com
ScienceDirect
Proceedings of the Combustion Institute 31 (2007) 2643–2652
Proceedings of the Combustion Institute
www.elsevier.com/locate/proci

Numerical study of thermal decomposition and pressure generation in charring solids undergoing opposed-flow flame spread

Won Chan Park [a,*], Arvind Atreya [a], Howard R. Baum [b]

[a] Department of Mechanical Engineering, University of Michigan, 2202 GGBL, 2250 Hayward St., Ann Arbor, MI 48109, USA
[b] National Institute of Standards and Technology, Building and Fire Research Laboratory, Gaithersburg, MD 20899, USA

Abstract

Thermal decomposition and pressure generation in charring solids undergoing opposed-flow flame spread have been numerically studied with a detailed physics-based model. The physical problem is modeled as a steady state two-dimensional process including three parallel finite rate reactions and volatiles convection. Local thermal equilibrium is assumed between char matrix and volatiles. For pressure calculation, the volatiles are assumed to follow the ideal gas law and Darcy's law. Numerical result indicates that the char density and product yields are functions of depth due to an insulating char layer. In addition, the characteristics of various simplifying assumptions such as global reaction, infinite rate kinetics and no convective gas transport have been investigated. The global reaction model shows excellent agreement on char layer thickness with the detailed model. However, it predicts higher pressure inside the charring solid. Infinite reaction rate model shows thicker char layer in the fore region and thinner char layer in the downstream region due to constant pyrolysis temperature. Also, it shows lower pressure in the char. Simplified energy model predicts thicker char and higher pressure than the detailed model.

Keywords: Flame spread; Charring material; Char; Wood; Pyrolysis

1. Introduction

Opposed-flow flame spread on a charring solid is an important mode of flame spread in a fire. Downward or horizontal flame spread against buoyancy induced air flow are familiar examples. Contrary to a vaporizing material, charring solid undergoes complex thermal decomposition resulting in an insulating char layer. This solid phase pyrolysis process governs volatile fuel generation and its transport to the flame above the charring solid. Numerous studies have been conducted on the subject of charring material pyrolysis. However, most of them focused on unsteady one-dimensional geometry [1,2] and only a few on the two-dimensional charring process occurring during flame spread [3,4]. Recently, an analytical model for opposed-flow flame spread over a charring solid was developed by Atreya and Baum [3] based on simplifying assumptions. Their model assumes infinite rate kinetics with constant pyrolysis temperature and no gas convective transport. Pressure generation inside the charring solid was not considered although it plays an

* Corresponding author. Fax: +1 734 647 3170.
E-mail address: wochpark@umich.edu (W.C. Park).

1540-7489/$ - see front matter © 2006 The Combustion Institute. Published by Elsevier Inc. All rights reserved.
doi:10.1016/j.proci.2006.08.096

Nomenclature

A	pre-exponential factor [s^{-1}]
B	permeability [m^2]
C	specific heat capacity [J/kg K]
E	activation energy [J/mol]
k	pyrolysis rate [s^{-1}]
L	length [m]
M	molecular weight [kg/mol]
n	normal to the interface
P	pressure [Pa]
P_i	partial pressure [Pa]
Q	reaction heat per unit mass of virgin solid [J/kg]
R	universal gas constant [J/mol K]
S	mass generation rate per unit volume [kg/m^3 s]
T	temperature [K]
t	time [s]
V	velocity [m/s]
Y	product yield
x, y	Cartesian coordinates [m]

Greek symbols

α	thermal diffusivity [m^2/s]
Δh	pyrolysis heat at reference temperature T_0
ε	porosity
λ	thermal conductivity [W/mK]
μ	dynamic viscosity [kg/ms]
ν	volatile fraction factor
η	degree of pyrolysis
Ω	entire domain [m^2]
ρ	apparent density [kg/m^3]
τ, ω	parabolic coordinates

Superscript

*	area integrated
-	non-dimensional

Subscripts

c	char
c0	final char
fs	flame spread
g	gas
if	interface
p	pyrolysis
s	surface
t	tar
v	volatiles
w	virgin solid
w0	initial virgin solid
x, y	Cartesian coordinates
0	reference

important role in fuel gas transport and structural damage caused by rupture and subsequent breakage of the structure member in a fire. While a few models have considered pressure generation during charring, pressure calculations were primarily used to provide convective gas flow information required for the thermal analysis. Note that in one-dimensional models often used, pressure generation is not required to determine the direction of gas flow. Consequently, few previous studies have focused on pressure generation during the charring process. Fredlund [5] measured pressure inside a wood block during the charring process and compared it with his numerical model. Staggs [1] developed a mathematical model for pressure in developing chars. He derived exact solutions for isothermal conditions in the char. Baum et al. [4] developed an analytical model for the transport of gases in a charring solid. This model solves for the gas pressure and temperature distributions in the char.

To prevent large computational burden or to make the charring problem analytically tractable, not all the detailed physical phenomena are accounted. Simplifications such as infinite rate kinetics, global reaction and no convective gas transport have been widely used in charring models. Since these simplifications inevitably affect the accuracy, it is important to assess their effects on the result especially when they are applied for fire safety applications. Thus, the objectives of this study are: (1) to numerically investigate the charring behavior and pressure generation in a charring solid during flame spread taking account of detailed physical processes, and (2) to assess the characteristics of simplified models by means of comparison with the detailed model.

2. Mathematical modeling

The schematic diagram of the physical problem is illustrated in Fig. 1. Flame spread on the top surface of a semi-infinite charring material is considered. A thin flame sheet which stretches from the flame inception point to downstream of the wind blowing over the charring material

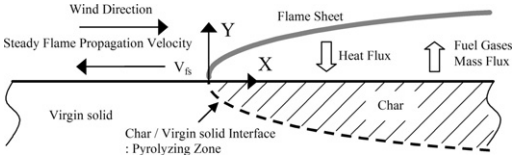

Fig. 1. Schematic of the physical problem: steady propagation of an opposed-flow diffusion flame on the surface of a charring solid.

advances against the wind at a constant speed V_{fs}. The origin of coordinates is fixed to the flame foot to render the flame spread as a steady process with the charring solid moving into the flame foot with the constant velocity V_{fs}. Heat flux coming from the flame sheet decreases downstream due to increasing distance between the flame sheet and char surface. On the other hand, heat conduction into the char decreases downstream as the char thickness increases. From these observations and the fact that radiation from the char surface increases nonlinearly with its temperature, it is reasonable to assume a constant temperature of the burning char surface ($x \geqslant 0$, $y = 0$). According to Atreya [6], the heat exchange between the gas phase and the solid phase across the upstream surface ($x < 0$, $y = 0$) is small. Therefore, adiabatic condition for upstream and constant surface temperature for downstream is used as the charring solid surface boundary condition. For pressure, ambient pressure boundary condition is applied at the char surface.

2.1. Reaction mechanism

A three-way parallel finite rate reaction model is used for detailed analysis. A global finite rate reaction model and an infinite rate reaction model are used to simulate simplified versions of the problem. Kinetic rate constants for finite rate models were taken from Di Blasi's experimental work [7] on beech wood.

For the three-way parallel finite rate reaction model, three primary product classes, which are char, tar and gas, are formed by the thermal decomposition of the virgin solid. Tar and gas represent condensable volatiles and non-condensable volatiles. Each product formation rate is controlled by its kinetic rate constants.

For the global finite rate reaction model, pyrolysis is modeled as a global decomposition reaction. Primary products are char and volatiles representing the sum of tar and gas. In contrast with the parallel reaction model, the product yield ratio between char and volatiles needs to be predetermined.

For the infinite rate reaction model, the charring solid is divided into two zones, char and virgin solid. The thermal decomposition of the virgin solid occurs abruptly at the interface between the two zones. The temperature along the interface is set to the constant pyrolysis temperature, T_p.

2.2. Conservation of mass and energy

(1) The detailed model

The steady state conservation of mass for each component inside the charring solid is described by the following equations:

Solid phase components:

$$\vec{\nabla} \cdot (\rho_w \vec{V}_{fs}) + \sum S_i = 0, \quad i = c, t, g \tag{1}$$

$$\vec{\nabla} \cdot (\rho_c \vec{V}_{fs}) - S_c = 0 \tag{2}$$

The volatiles in pore are assumed to be ideal gases and to follow Darcy's law.

$$\vec{\nabla} \cdot \left(\rho_j \frac{B}{\mu} \vec{\nabla} P \right) - \vec{\nabla} \cdot (\varepsilon \rho_j \vec{V}_{fs}) + S_j = 0, \quad j = t, g \tag{3}$$

Where, P is the sum of partial pressures, $P = \sum P_j$, $j = t, g$

Thermal decomposition kinetics is modeled as a first order Arrhenius reaction, the pyrolysis rate $k_i = A_i e^{-\frac{E_i}{RT}}$. Each product generation rate is described as follows:

$$S_i = k_i \rho_w, \quad i = c, t, g \tag{4}$$

The steady state conservation of energy with local thermal equilibrium assumption between volatiles and porous solid is described by:

$$\vec{\nabla} \cdot (\lambda \vec{\nabla} T) - \left(\sum \rho_i C_i + \varepsilon \sum \rho_j C_j \right) \vec{V}_{fs} \cdot \vec{\nabla} T + \sum \rho_j C_j \frac{B}{\mu} \vec{\nabla} P \cdot \vec{\nabla} T + Q = 0, \quad i = w, c, \ j = t, g \tag{5}$$

Reaction heat is a function of temperature. It is given by:

$$Q(T) = (T - T_0) \sum S_i (C_w - C_i) - \Delta h \sum S_i, \quad i = c, t, g \tag{6}$$

Porosity is defined as a function of solid phase density as follows:

$$\varepsilon = 1 - (1 - \varepsilon_w) \frac{\rho_w + \rho_c}{\rho_{w0}} \tag{7}$$

Viscosity of the volatiles is modeled as a linear function of temperature as $\mu = \mu_p \, (T/T_p)$. Thermal conductivity and permeability are modeled as linearly interpolated between virgin solid and char. By combining Eq. (3) and the equation of state, the pressure equation of tar and gas can be obtained as follows:

$$\vec{\nabla} \cdot \left(\frac{B P_j}{\mu T} \vec{\nabla} P \right) - \vec{\nabla} \left(\frac{\varepsilon P_j}{T} \right) \cdot \vec{V}_{fs} + \frac{R}{M_j} S_j = 0, \quad j = t, g \tag{8}$$

The energy equation is derived from Eq. (5) as follows:

$$\vec{\nabla}\cdot(\lambda\vec{\nabla}T)-\left(\sum\rho_i C_i+\frac{\varepsilon}{RT}\sum M_j P_j C_j\right)\vec{V}_{\mathrm{fs}}\cdot\vec{\nabla}T+\frac{\sum M_j P_j C_j}{RT}\frac{B}{\mu}\vec{\nabla}P\cdot\vec{\nabla}T+Q=0,\quad i=\mathrm{w},\mathrm{c},\ j=\mathrm{t},\mathrm{g} \tag{9}$$

(2) The global reaction model

Pressure and energy equations for global reaction are described as follows,

$$\vec{\nabla}\cdot\left(\frac{BP}{\mu T}\vec{\nabla}P\right)-\vec{\nabla}\left(\frac{\varepsilon P}{T}\right)\cdot\vec{V}_{\mathrm{fs}}-v\frac{R}{M_{\mathrm{v}}}S_{\mathrm{w}}=0 \tag{10}$$

where, virgin solid decomposition rate is $S_{\mathrm{w}}=-k_{\mathrm{w}}\rho_{\mathrm{w}}$ and v is predetermined volatile fraction factor.

$$\vec{\nabla}\cdot(\lambda\vec{\nabla}T)-\left(\rho_{\mathrm{w}}C_{\mathrm{w}}+\rho_{\mathrm{c}}C_{\mathrm{c}}+\varepsilon C_{\mathrm{v}}\frac{M_{\mathrm{v}}P}{RT}\right)\vec{V}_{\mathrm{fs}}\cdot\vec{\nabla}T+C_{\mathrm{v}}\frac{M_{\mathrm{v}}P}{RT}\frac{B}{\mu}\vec{\nabla}P\cdot\vec{\nabla}T+Q=0 \tag{11}$$

(3) The infinite rate reaction model

For the infinite rate model, variables and properties become constant such as $\rho_{\mathrm{c}}=\rho_{\mathrm{c0}}$, $\rho_{\mathrm{w}}=\rho_{\mathrm{w0}}$, $\varepsilon=\varepsilon_{\mathrm{c}}$ or ε_{w}, $\lambda=\lambda_{\mathrm{c}}$ or λ_{w} and $B=B_{\mathrm{c}}$ in char or virgin solid. Since volatiles are generated along the interface and most of them travel through the char layer to the surface, the virgin solid can be modeled as impermeable and the pressure equation is solved only inside the char. Thus, energy equation for virgin solid is reduced from Eq. (9) to following expression.

$$\alpha_{\mathrm{w}}\nabla^2T-\vec{V}_{\mathrm{fs}}\cdot\vec{\nabla}T=0 \tag{12}$$

where, virgin solid thermal diffusivity is $\alpha_{\mathrm{w}}=\lambda_{\mathrm{w}}/(\rho_{\mathrm{w0}}\ C_{\mathrm{w}})$.

The conservation of energy in char considering volatiles flow is described as follows:

$$\lambda_{\mathrm{c}}\nabla^2T-\left(\rho_{\mathrm{c0}}C_{\mathrm{c}}+\varepsilon_{\mathrm{c}}C_{\mathrm{v}}\frac{M_{\mathrm{v}}P}{RT}\right)\vec{V}_{\mathrm{fs}}\cdot\vec{\nabla}T+C_{\mathrm{v}}\frac{M_{\mathrm{v}}P}{RT}\frac{B_{\mathrm{c}}}{\mu}\vec{\nabla}P\cdot\vec{\nabla}T=0 \tag{13}$$

The energy balance among conduction heat fluxes for both virgin solid and char and the reaction heat of thermal decomposition gives the char–virgin solid interface condition (Stefan condition).

$$\lambda_{\mathrm{c}}\vec{\nabla}T|_{\mathrm{c}}-\lambda_{\mathrm{w}}\vec{\nabla}T|_{\mathrm{w}}+\vec{V}_{\mathrm{fs}}\rho_{\mathrm{w0}}Q=0;\quad T=T_{\mathrm{p}} \tag{14}$$

Since there is no volatile generation inside the char, Eq. (8) can be reduced as follows:

$$\vec{\nabla}\cdot\left(\frac{B_{\mathrm{c}}P}{\mu T}\vec{\nabla}P\right)-\vec{\nabla}\left(\frac{\varepsilon_{\mathrm{c}}P}{T}\right)\cdot\vec{V}_{\mathrm{fs}}=0 \tag{15}$$

Mass balance at the interface is given by the following expression:

$$(\rho_{\mathrm{w0}}-\rho_{\mathrm{c0}})V_{\mathrm{fs}}n_x=\varepsilon_{\mathrm{c}}\rho_{\mathrm{v}}V_{\mathrm{fs}}n_x-\rho_{\mathrm{v}}\frac{B_{\mathrm{c}}}{\mu}\frac{\partial P}{\partial n}\bigg|_{\mathrm{if}} \tag{16}$$

where, n_x is the x-direction component of the interface normal vector $\vec{n}$.

(4) The simplified energy model

By neglecting the convective volatile transport in a charring solid, the energy equation does not contain pressure related terms. This approach eliminates the difficulty of solving the pressure equation. This simplified energy model is convenient especially when only the thermal process is of interest.

In this model, Eqs. (9) and (11) reduces as follows:

$$\vec{\nabla}\cdot(\lambda\vec{\nabla}T)-(\rho_{\mathrm{w}}C_{\mathrm{w}}+\rho_{\mathrm{c}}C_{\mathrm{c}})\vec{V}_{\mathrm{fs}}\cdot\vec{\nabla}T+Q=0 \tag{17}$$

For infinite rate model, Eq. (13) reduces as below:

$$\alpha_{\mathrm{c}}\nabla^2T-\vec{V}_{\mathrm{fs}}\cdot\vec{\nabla}T=0 \tag{18}$$

where, thermal diffusivity of char is $\alpha_{\mathrm{c}}=\lambda_{\mathrm{c}}/(\rho_{\mathrm{c0}}\ C_{\mathrm{c}})$.

3. Numerical results and discussion

The mathematical models presented here were solved by numerical methods based on the finite volume method for finite rate reaction models, and the finite difference method was used with the front tracking method developed by Jung et al. [8,9] for infinite rate reaction models. Numerical analysis was performed on six cases with various combinations of kinetics and energy models. These are summarized in Table 1.

The physical dimensions of computational domain are $-0.025\ \mathrm{m}\leqslant x\leqslant 0.1\ \mathrm{m}$ $(-71.5\leqslant\bar{x}\leqslant 286.1)$ and $-0.015\ \mathrm{m}\leqslant y\leqslant 0\ \mathrm{m}$ $(-42.9\leqslant\bar{y}\leqslant 0)$.

Table 1
Numerical analysis conditions

Case 1a	Parallel reactions and detailed energy equation
Case 1b	Parallel reactions and simplified energy equation
Case 2a	Global reaction and detailed energy equation
Case 2b	Global reaction and simplified energy equation
Case 3a	Infinite rate reaction and detailed energy equation
Case 3b	Infinite rate reaction and simplified energy equation
Case 4	Analytical model [3,4]

Table 2
Properties and kinetic constants

Property	Value	Source
ρ_{w0}	700 kg/m^3	[2]
ρ_{c0}	92.8 kg/m^3	Calculated
C_w	1.5 kJ/kg K	[11]
C_c	1.1 kJ/kg K	[11]
C_t	2.5 kJ/kg K	[10]
C_g	1.1 kJ/kg K	[10]
C_v	2.287 kJ/kg K	Calculated
ε_w	0.4	[10]
E_c	111.7 kJ/mol	[7]
E_t	148.0 kJ/mol	[7]
E_g	152.7 kJ/mol	[7]
E_w	141.2 kJ/mol	[7]
A_c	3.27×10^6 s^{-1}	[7]
A_t	1.08×10^{10} s^{-1}	[7]
A_g	4.38×10^9 s^{-1}	[7]
A_w	4.38×10^9 s^{-1}	[7]
Δh	430 kJ/kg	[7]
M_g	0.038 kg/mol	[10]
M_t	0.11 kg/mol	[10]
M_v	0.0854 kg/mol	Calculated
μ_p	2.3×10^{-5} kg/ms	[2]
B_w	1.0×10^{-16} m^2	[10]
B_c	1.0×10^{-13} m^2	[10]
λ_w	0.367 W/m K	[2]
λ_c	0.708 W/m K	[2]
V_{fs}	0.001 m/s	[3]
R	8.314 J/mol K	
T_p	696.63 K	Calculated
T_s	850 K	[6]
T_0	300 K	

The coordinate 'x' represents the distance from the flame foot and 'y' indicates the depth from the surface. Non-dimensional coordinate variables are defined by $\bar{x} = xV_{fs}/\alpha_w$ and $\bar{y} = yV_{fs}/\alpha_w$. Uniform 300×180 meshes were used for numerical computation. The material properties and constants used for computations are listed in Table 2.

3.1. Temperature and pressure

Temperature $\bar{T} = (T - T_0)/(T_s - T_0)$ distribution of *case 1a* appears in Fig. 2. The steep slope of iso-temperature lines near $x = 0$ indicates that a relatively larger amount of pyrolysis occurs near the flame foot than in the downstream region. In addition, a larger temperature gradient near $x = 0$ means the thinner pyrolysis zone than that of downstream region. In spite of a higher thermal conductivity of the char than that of the virgin solid, it is difficult to observe the temperature gradient difference between the char and the virgin solid regions because a portion of the thermal energy conducted through the char is absorbed by endothermic reaction in the pyrolysis zone and smaller heat conduction exists in the unpyrolyzed region. Here, the thermal conductivities of the virgin solid and char are taken at average temperatures during the charring process; 500 K for virgin solid and 770 K for char. Large char conductivity is attributed to a strong radiation effect inside the char pores at high temperature. Fig. 3 shows pressure $\bar{P} = P/P_0$ distribution inside the char and pyrolysis zone. To reduce computational time, pressure equation was computed for the char and pyrolysis zones which are pyrolyzed in excess of 0.1%. The virgin solid ($\eta < 0.1\%$; here, $\eta = 1 - \rho_w/\rho_{w0}$) is assumed as impermeable. The pressure rises with depth up to $\bar{P} = 1.12$ which covers char and most of the pyrolysis zone. The pressure in the char region ($1.0 < \bar{P} < 1.07$) increases linearly with depth because the volatile mass flow rate and the permeability are nearly constant. In the pyrolysis zone ($1.07 < \bar{P} < 1.12$), although the volatile mass flow rate decreases with the depth depending on η, the pressure shows nearly linear increase with depth due to the permeability variation from char to virgin solid. The deep region ($\bar{P} > 1.12$) shows a insignificant pressure variation due to the negligible volatiles generation and volatile flow rate. This observation validates the impermeable virgin solid assumption.

3.2. Products yields

Figure 4 shows that char density increases with depth in the completely pyrolyzed region, i.e., char.

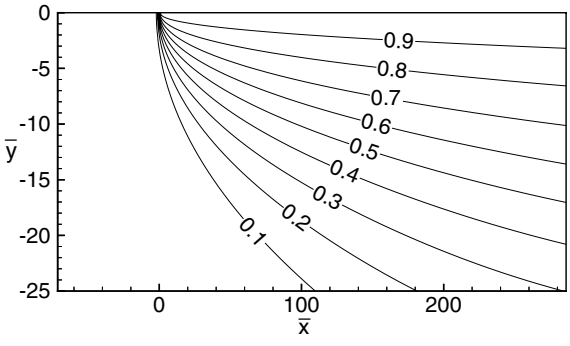

Fig. 2. Temperature profiles $\bar{T} = \frac{T-T_0}{T_s-T_0}$; *case 1a*.

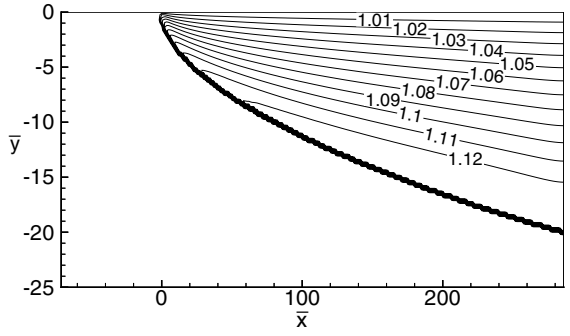

Fig. 3. Pressure $\bar{P} = \frac{P}{P_0}$ profiles; *case 1a*.

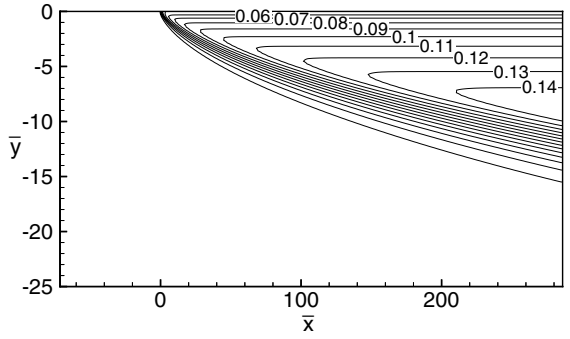

Fig. 4. Char density $\bar{\rho}_c = \frac{\rho_c}{\rho_{w0}}$ distribution; *case 1a*.

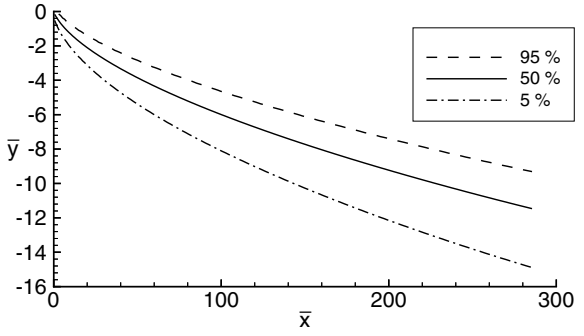

Fig. 5. Profiles of the degree of pyrolysis for $\eta = 1 - \frac{\rho_w}{\rho_{w0}}$, $\eta = 5\%$, 50%, 95%; *case 1a*.

Near the surface, pyrolysis occurs at high temperature and at high heating rate resulting in high volatiles yield, whereas, in the deeper regions more char is formed due to the pyrolysis at lower temperature and heating rate. The pyrolysis reaction zone can be recognized by the band of iso-char density profiles underneath the char region. The pyrolysis zone approximately matches the area between $\eta = 5\%$ and $\eta = 95\%$ in Fig. 5. Figure 6 shows the char yield ratio defined by $S_c/(S_c + S_t + S_g)$ at $x = 0.09$ m. Char yield of *case 1a*, *1b* increases rapidly in the deeper region. Product generation rates defined by $\int_{-L_y}^{0} S_i \mathrm{d}y / \frac{1}{L_x} \int_0^{L_x} \int_{-L_y}^{0} (S_c + S_t + S_g)\mathrm{d}y\mathrm{d}x$; $i = $ c, t, g; $L_x = 0.1$m; $L_y = 0.015$m are shown in Fig. 7. All the three production rates show a peak near $\bar{x} = 0$ and decrease rapidly until $\bar{x} = 20$ and then decrease gradually. The pyrolysis rate decreases in the downstream region because heat conduction from the surface to the pyrolysis zone is reduced due to a thicker char layer.

The tar production rate is one order of magnitude larger than the other two products. The

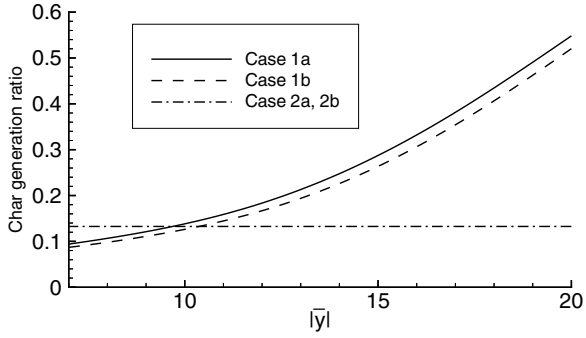

Fig. 6. Char yield ratio $\frac{S_c}{S_c+S_t+S_g}$ at $x = 0.09$ m ($\bar{x} = 257.5$).

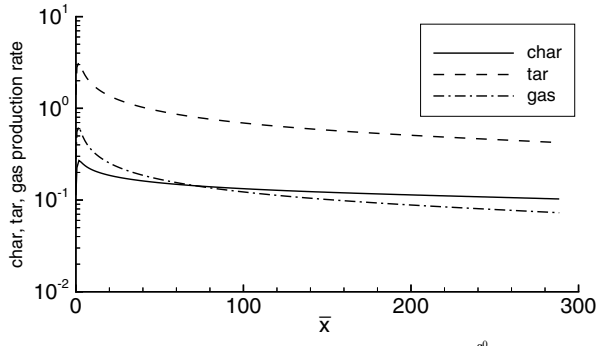

Fig. 7. Comparison of products generation defined by $\frac{\int_{-L_y}^{0} S_i \mathrm{d}y}{\frac{1}{L_x}\int_0^{L_x}\int_{-L_y}^{0}(S_c+S_t+S_g)\mathrm{d}y\mathrm{d}x}$; $i = \mathrm{c}, \mathrm{t}, \mathrm{g}$.

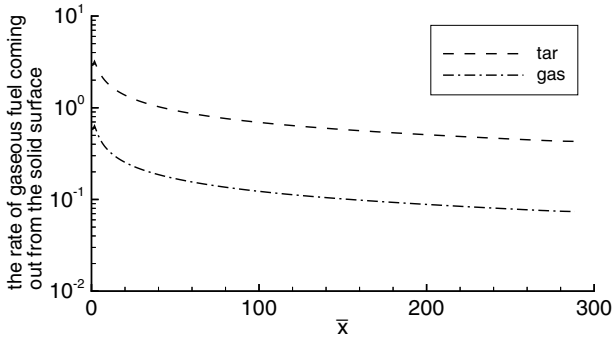

Fig. 8. The rate of gaseous fuel coming out from the solid surface defined by $\frac{V_{y,s}\rho_{i,s}}{\frac{1}{L_x}\int_0^{L_x}\int_{-L_y}^{0}(S_c+S_t+S_g)\mathrm{d}y\mathrm{d}x}$; $i = \mathrm{t}, \mathrm{g}$.

gas production rate is larger than the char production rate for $\bar{x} < 70$ and then the trend reverses for $\bar{x} > 70$. This is consistent with higher char densities observed deeper inside the solid.

The rate of gaseous fuel coming out from the solid surface is shown in Fig. 8. Since the ratio of char length to char depth is very large, the gaseous fuel ejection distributions in Fig. 8 is almost the same as the volatile generation rate as Fig. 7.

Both the global reaction model and the infinite rate model need a product yield ratio as an input parameter, i.e., volatile fraction '*v*'. The value was found based on the numerical result of *case 1a* by the integration of each product generation rate over the entire computational domain using Eqs. (19) and (20). The products' mass yield fractions

are: char 13.3%, tar 73.5% and gas 13.2%. This result gives $v = 0.867$.

$$S_i^* = \int_\Omega S_i \mathrm{d}A, \quad i = \mathrm{c,t,g} \tag{19}$$

$$Y_i^* = \frac{S_i^*}{\sum S_j^*}, \quad i = \mathrm{c,t,g},\ j = \mathrm{c,t,g} \tag{20}$$

3.3. Pyrolysis temperature

The infinite rate model needs a constant pyrolysis temperature 'T_p' as an input parameter. Though using proper pyrolysis temperature is important for the infinite rate model, how to determine the pyrolysis temperature has not been clearly established in previous research. In this work, the pyrolysis temperature was determined by energy balance from the numerical result of *case 1a*. To match the energy balance between *case 1a* and the infinite rate model, the reaction heat 'Q' should be the same for both models. Based on this relation, the pyrolysis temperature can be found by Eq. (21) and the value is $T_\mathrm{p} = 696.6$ K

$$T_\mathrm{p} = \frac{\int_\Omega (T - T_0) \sum S_i (C_\mathrm{w} - C_i) \mathrm{d}A}{\sum S_i^* (C_\mathrm{w} - C_i)} + T_0, \quad i = \mathrm{c,t,g} \tag{21}$$

3.4. Simplified models: char layer thickness

The interfaces between virgin solid and char of simplified models are compared with the detailed model in Fig. 9. The finite rate models show a gradual transition from virgin solid to char instead of a discontinuous interface of the infinite rate model. For the comparison, $\eta = 50\%$ line is regarded as char–virgin solid interface for finite rate models. The global reaction model (*case 2a*, *2b*) shows excellent agreement with the parallel reaction model (*case 1a*, *1b*) in char layer thickness. The infinite rate model predicts a thicker char layer in the flame foot near region ($\bar{x} < 120$) and then a thinner layer in far downstream region ($\bar{x} > 120$) because pyrolysis of the finite rate models starts at high temperature due to a fast heating rate near $\bar{x} = 0$ and then proceeds for lower temperature due to a slower heating rate by increasing the char layer thickness. The simplified energy model (*case 1b*, *2b*, *3b*) predicts approximately 10% thicker char layers than the detailed energy model because no gas convective transport simplification does not account for the loss of thermal energy carried by the volatiles leaving the surface at T_s. However, modification of the thermal properties of char such as conductivity can be considered to improve the accuracy of the simplified energy model.

3.5. Simplified models: pressure

The non-dimensional pressure profiles defined by $\bar{P} = P/P_0$ at $x = 0.09$ m ($\bar{x} = 257.5$) are shown in Fig. 10. The infinite rate model predicts lower pressure than the finite rate models. The pyrolysis rate can be interpreted from the virgin solid–char interface slope. Except for the very beginning part ($\bar{x} < 30$), the interface slopes of the infinite reaction rate models are smaller than those of

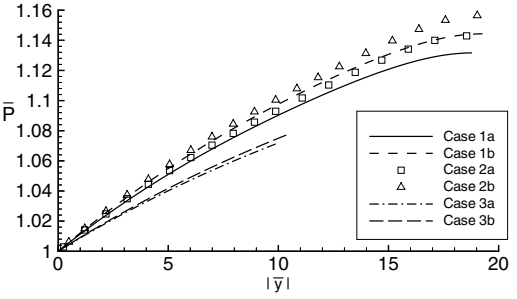

Fig. 10. Comparison of pressure at $x = 0.09$ m ($\bar{x} = 257.5$).

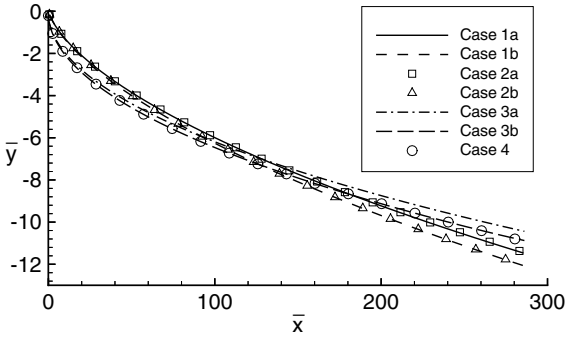

Fig. 9. Comparison of virgin solid/char interface.

the finite rate models (Fig. 9). Thus, the finite rate models show more volatile generation and a higher pressure rise for the domain $\bar{x} > 30$. The pressure profiles of the infinite rate model end at about $|\bar{y}| = 11$ which corresponds to the interface. The finite rate models show that the pressure rise is maintained until $|\bar{y}| = 18$ and then the pressure rise drops down gradually to zero. The global reaction model shows 8.5% higher pressure than the detailed reaction model at the deep zone because the detailed reaction model predicts a higher char yield than the global reaction model which has a constant char yield ratio for $|\bar{y}| > 10$ (Fig. 6). The simplified energy model predicts a 9% higher pressure than the detailed energy model due to a higher pyrolysis rate as mentioned in the char depth comparison.

3.6. Comparison with the analytical model

For the purpose of validating the numerical model, the numerical result was compared with the analytical model which has been developed by Baum and Atreya [3,4]. Since the analytical model is based on infinite rate kinetics and the simplified energy model, the numerical result of *case 3b* can be directly compared. *Case 4* and *case 3b* show excellent agreement in char depth and pressure profile in Figs. 9 and 11. The parabolic variable ω_c in Fig. 11 is defined by the parabolic coordinate transformation $\omega_c = \omega\sqrt{\frac{\alpha_w}{\alpha_c}}$ and

$$\tau + i\omega = \sqrt{\frac{2V_{fs}}{\alpha_w}}(x + iy)[3]. \tag{22}$$

3.7. Computational time

The relative computation times for the models were *case 1a* 1.0; *case 1b* 0.45; *case 2a* 0.15, *case 2b* 0.20; *case 3a* 0.87; *case 3b* 1.87. Global reaction model (*case 2*) was the fastest because its' simple reaction kinetics reduces the computational burden. Interestingly, the infinite reaction model (*case 3*) took large computational time compared with simple kinetics due to the large numerical effort required to track the interface between the virgin solid and the char.

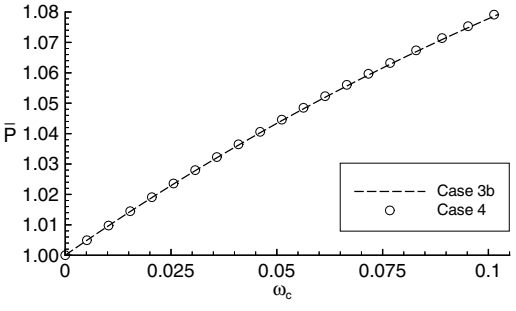

Fig. 11. Dimensionless pressure $\bar{P}$ plotted versus the parabolic coordinate ω_c which represents depth and is derived from the parabolic coordinates transformation defined by Eq. (22).

4. Conclusions

The thermal decomposition and pressure generation in charring solids undergoing opposed-flow flame spread have been numerically studied with detailed physics and chemistry. In addition, the characteristics of various simplified models have been investigated. It was found that: (i) A larger amount of pyrolysis occurs near the flame foot than in the downstream region and the pyrolysis zone is thinner near $x = 0$ than in the downstream region. (ii) The temperature gradient does not vary significantly from char to virgin solid because the endothermic reaction heat partly offsets the larger thermal conductivity of char. (iii) The pressure rises with depth in char and the pyrolysis zone and then becomes constant in the virgin solid. This observation validates the impermeable virgin solid assumption. (iv) The char density increases with depth because the pyrolysis occurs at a lower temperature in the deeper region. (v) The averaged products yield mass fractions are: char 13.3%, tar 73.5% and gas 13.2% and the pyrolysis temperature, found by energy balance, is $T_p = 696.6$ K. (vi) The global reaction model shows excellent agreement with the parallel reaction models in the char layer thickness. However, it predicts a higher pressure inside the char and pyrolysis zones. (vii) The infinite reaction rate model predicts a thicker char layer in the flame foot near region and a thinner char layer in the downstream region due to a constant pyrolysis temperature. It also shows lower pressure in the char. (viii) The simplified energy model predicts thicker char and higher pressure than the detailed energy model. However, modification of thermal properties such as conductivity of char can be considered to improve its accuracy.

Acknowledgments

The first author thanks Professor M.M. Chen (University of Michigan, Ann Arbor) for his advice on the front tracking finite difference method. This research was funded by NIST Grant # 3D1086.

References

[1] J.E.J. Staggs, *Poly. Degrad. Stab.* 82 (2003) 297–307.

[2] A. Galgano, C. Di Blasi, *Ind. Eng. Chem. Res.* 42 (2003) 2101–2111.
[3] A. Atreya, H.R. Baum, *Proc. Combust. Inst.* 29 (2002) 227–236.
[4] H.R. Baum, A. Atreya, in: Proc. Joint Meeting of U.S. Sect. Combust. Inst., Philadelphia, PA 2005.
[5] B. Fredlund, *A model for heat and mass transfer in timber structure during fire*, Ph.D. thesis, Lund University, Sweden, 1988.
[6] A. Atreya, *Pyrolysis, ignition and flame spread on horizontal surfaces of wood*, Ph.D. thesis, Harvard University, Cambridge, MA, 1983.
[7] C. Di Blasi, C. Branca, *Ind. Eng. Chem. Res.* 40 (2001) 5547–5556.
[8] J.Y. Jung, H. Lee, M.M. Chen, *Num. Heat Trans. Part B* 45 (2004) 421–448.
[9] J.Y. Jung, *Numerical simulation of alloy solidification*, Ph.D. thesis, University of Michigan, Ann Arbor, MI, 2000.
[10] M.G. Gronli, *A theoretical and experimental study on the thermal degradation of biomass*, Ph.D. thesis, NTNU, Trondheim, Norway, 1996.
[11] C. Di Blasi, *Chem. Eng. Sci.* 31 (7) (1996) 1121–1132.

Comment

Kazunori Duwana, University of Kentucky, USA. Your study showed the importance of finite rate chemistry for better prediction. Is it possible to improve your analytical model to consider finite rate chemistry?

Reply. We do not know if the model with finite rate chemistry can be analytically solved. However, it appears that the treatment of the Arrhenius expression will be difficult. The real question is: ''What level of chemical detail is necessary to reproduce the experimentally observed phenomena (pyrolysis temperature model (zero-step), single-step decomposition, or multi-step decomposition)?'' While this cannot be answered without experimental data, a few things are obvious: (i) In the pyrolysis temperature model, it is necessary to make two assumptions – (a) the value of the pyrolysis temperature and (b) the fraction of the material converted to char (char yield). (ii) In the single-step decomposition model, only one assumption is necessary – the char yield. (iii) In the multi-step model, no assumptions are needed. Finally, there is a question of how many steps in the multi-step chemistry model and how to determine the Arrhenius constants?

The difficulty with the pyrolysis temperature and one-step chemistry models is that 'pyrolysis temperature' and 'char yield' are not constants. An alternate approach is to determine the best value of the 'pyrolysis temperature' and 'char yield' for a given problem consistent with the known chemistry for use in the analytical solution. We are currently in the process of completing this analysis and making experimental measurements.